

BLACK HOLE AND NEUTRON STAR BINARY MERGERS IN TRIPLE SYSTEMS: II. MERGER ECCENTRICITY AND SPIN-ORBIT MISALIGNMENT

BIN LIU¹, DONG LAI¹, YI-HAN WANG²

¹ Cornell Center for Astrophysics and Planetary Science, Cornell University, Ithaca, NY 14853, USA

² Department of Physics and Astronomy, Stony Brook University, Stony Brook, NY 11794-3800, USA

Draft version August 14, 2019

ABSTRACT

We study the dynamical signatures of black hole (BH) and neutron star (NS) binary mergers via Lidov-Kozai oscillations induced by tertiary companions in hierarchical triple systems. For each type of binaries (BH-BH and BH-NS), we explore a wide range of binary/triple parameters that lead to binary mergers, and determine the distributions of merger time T_m , eccentricity (e_m) and spin-orbit misalignment angle (θ_{sl}^f) when the binary enters the LIGO/VIRGO band (10 Hz). We use the double-averaged (over both orbits) and single-averaged (over the inner orbit) secular equations, as well as N-body integration, to evolve systems with different hierarchy levels, including the leading-order post-Newtonian effect, de-Sitter spin-orbit coupling and gravitational radiation. We find that for merging BH-BH binaries with comparable masses, about 7% have $e_m > 0.1$ and 0.7% have $e_m > 0.9$. The majority of the mergers have significant eccentricities in the LISA band. The BH spin evolution and the final spin-orbit misalignment θ_{sl}^f are correlated with the orbital evolution and e_m . Mergers with negligible e_m ($\lesssim 10^{-3}$) have a distribution of θ_{sl}^f that peaks around 90° (and thus favoring a projected binary spin parameter $\chi_{\text{eff}} \sim 0$), while mergers with larger e_m have a more isotropic spin-orbit misalignments. For typical BH-NS binaries, strong octupole effects lead to more mergers with non-negligible e_m (with $\sim 18\%$ of the mergers having $e_m > 0.1$ and 2.5% having $e_m > 0.9$), and the final BH spin axis tends to be randomly orientated. Measurements or constraints on eccentric mergers and θ_{sl}^f from LIGO/VIRGO and LISA would provide useful diagnostics on the dynamical formation of merging BH or NS binaries in triples. The recently detected BH merger events may implicate such dynamical formation channel.

Subject headings: binaries: general - black hole physics - gravitational waves - stars: black holes - stars: kinematics and dynamics

1. INTRODUCTION

Recent studies (e.g., Miller & Hamilton 2002; Wen 2003; Thompson 2011; Antonini & Perets 2012; Silsbee & Tremaine 2017; Antonini et al. 2017; Liu & Lai 2017, 2018; Hoang et al. 2018; Rodriguez & Antonini 2018) have suggested that tertiary-induced merger via Lidov-Kozai (LK) oscillations (Lidov 1962; Kozai 1962; Naoz 2016) may play a significant role in producing black-hole (BH) binaries detected by the LIGO/VIRGO collaboration (e.g., Abbott et al. 2016a,b, 2017a,b,c,d, 2018a,b). Merging BH and neutron star (NS) binaries can be formed efficiently in triple systems with the aid of a tertiary body that moves on an inclined (outer) orbit relative to the orbit of the inner (BH or NS) binary. The efficiency of the merger can be further enhanced when the triple is part of a quadruple system (e.g., when the tertiary component is itself a binary; see Fang et al. 2018; Liu & Lai 2019; Zevin et al. 2019; Fragione & Kocsis 2019) or more generally, when the outer orbit experiences quasi-periodic external forcing (e.g., Hamers & Lai 2017; Petrovich & Antonini 2017; Fragione et al. 2019).

Given the expected large number of BH mergers to be detected by LIGO/VIRGO in the coming years, it will be important to distinguish tertiary-induced merg-

ers from other dynamical BH binary formation channels (such as those involving close encounters in dense stellar clusters; e.g., Portegies Zwart & McMillan 2000; Miller & Lauburg 2009; O’Leary et al. 2006; Banerjee et al. 2010; Downing et al. 2010; Rodriguez et al. 2015; Chatterjee et al. 2017; Samsing et al. 2018) and the more traditional isolated binary channel (e.g., Lipunov et al. 1997, 2017; Podsiadlowski et al. 2003; Belczynski et al. 2010, 2016; Dominik et al. 2012, 2013, 2015), as well as the chemically homogeneous evolution channel (e.g., Mandel & de Mink 2016; Marchant et al. 2016) and gas-assisted mergers (e.g., Bartos et al. 2017). One possible indicator is the merger eccentricity: It has been noted that dynamical binary-single interactions in dense cluster (e.g., Samsing & Ramirez-Ruiz 2017; Rodriguez et al. 2018; Samsing & D’Orazio 2018; Fragione & Bromberg 2019) or in galactic triples (Silsbee & Tremaine 2017; Antonini et al. 2017; Fragione & Loeb 2019) may lead to BH binaries entering the LIGO band with modest or large eccentricities, although the fraction of such eccentric mergers is highly uncertain. Another potentially valuable observable is the BH spin, which carries information on the BH binary formation history. In particular, through the binary inspiral waveform, the mass-weighted projec-

tion of BH spin, $\chi_{\text{eff}} \equiv (m_1 \boldsymbol{\chi}_1 + m_2 \boldsymbol{\chi}_2)/(m_1 + m_2) \cdot \hat{\mathbf{L}}$, can be directly measured [here $m_{1,2}$ are the BH masses, $\boldsymbol{\chi}_{1,2} = c \mathbf{S}_{1,2}/(Gm_{1,2}^2)$ are the dimensionless BH spins, and $\hat{\mathbf{L}}$ is the unit orbital angular momentum vector of the BH binary]. While isolated binary evolution tends to generate approximately aligned BH spins (with respect to the orbit), and cluster dynamics tends to generate random spin orientations, recent works (Liu & Lai 2017, 2018; Antonini et al. 2018; Rodriguez & Antonini 2018) have shown that merging BH binaries produced in hierarchical triples may exhibit rich behaviors in spin-orbit orientations. For initially close BH binaries (with semi-major axis $a_0 \lesssim 0.2\text{AU}$), which may merge by themselves without the aid of a tertiary companion, modest ($\lesssim 20^\circ$) spin-orbit misalignments can be produced (e.g., Liu & Lai 2017) due to the perturbation of the tertiary companion. For wide binaries (with $a_0 \gtrsim 10\text{AU}$), a range of final spin-orbit misalignment angles θ_{sl}^f can be produced as the merging binary enters the LIGO band (Liu & Lai 2018): When the BHs have comparable masses (the octupole effect is thus negligible), the distribution of θ_{sl}^f is peaked around 90° ; when the two members of inner binary have highly unequal masses and the tertiary companion moves on an eccentric orbit, a more isotropic distribution of final spin axis is produced. Overall, merging BH binaries produced by Lidov-Kozai oscillations in triples exhibit a unique distribution of the effective (mass-weighted) spin parameter χ_{eff} .

In this paper, we extend our recent studies (Liu & Lai 2017, 2018) by exploring a wide range of triple systems. In particular, for a given merging compact binary with known masses, we examine all possible triple configurations and parameters that lead to binary mergers and determine the distributions of various merger properties (merger times, eccentricities and spin-orbit misalignments). We consider two sets of binary masses: $(m_1, m_2) = (30M_\odot, 20M_\odot)$ representing a canonical BH-BH binary, and $(30M_\odot, 1.4M_\odot)$ representing a canonical BH-NS binary. Our previous works focused on fully hierarchical triples, where either double-averaged (over both the inner and outer orbits) or single-averaged (over only the inner orbit) secular approximation is valid. The spin evolution was only studied for systems where the double-average approximation is valid [this is also the case for the study by Antonini et al. (2018) and Rodriguez & Antonini (2018)]. In this paper we examine systems with various levels of hierarchy, using both double-averaged and single-averaged secular equations, as well as direct N-body integrations to evolve the systems. This allows us to determine reliably the fraction of merging binaries that enter the LIGO band with appreciable eccentricities. In addition, unlike previous works, we consider systems where the initial BH spin and orbital axes are not perfectly aligned and we determine the distribution of the “final” spin-orbit misalignment angles θ_{sl}^f .

Our paper is organized as follows. In Section 2, we introduce three approaches to evolve the triple systems with different levels of approximation, including the de-

Sitter spin-orbit coupling effect. In Section 3, we perform a large set of numerical integrations, focusing on two types of stellar mass binaries (BH-BH and BH-NS), with imperfectly aligned initial spin axes. We compute the distributions of binary eccentricities and spin-orbit misalignments for systems that evolve into the LIGO band. We summarize our main results in Section 4.

2. THREE APPROACHES FOR TRIPLE EVOLUTION WITH SPIN-ORBIT COUPLING

2.1. Summary of Parameter Regimes

We consider a hierarchical triple system, composed of an inner BH binary of masses m_1, m_2 and a distant companion of mass m_3 that moves around the center of mass of the inner bodies. The reduced mass for the inner binary is $\mu \equiv m_1 m_2 / m_{12}$, with $m_{12} \equiv m_1 + m_2$. Similarly, the outer binary has $\mu_{\text{out}} \equiv (m_{12} m_3) / m_{123}$ with $m_{123} \equiv m_{12} + m_3$. The semi-major axes and eccentricities are denoted by a, a_{out} and e, e_{out} , respectively. Therefore, the orbital angular momenta of two orbits are given by $\mathbf{L} = L \hat{\mathbf{L}} = \mu \sqrt{G m_{12} a (1 - e^2)} \hat{\mathbf{L}}$ and $\mathbf{L}_{\text{out}} = L_{\text{out}} \hat{\mathbf{L}}_{\text{out}} = \mu_{\text{out}} \sqrt{G m_{123} a_{\text{out}} (1 - e_{\text{out}}^2)} \hat{\mathbf{L}}_{\text{out}}$. We define the mutual inclination between \mathbf{L} and \mathbf{L}_{out} (inner and outer orbits) as I .

To study the evolution of the inner binary under the influence of the tertiary companion, we use three approaches: the double-averaged (averaging over both the inner and outer orbits), and single-averaged (only averaging over the inner orbital period) secular equations of motion, as well as the direct N-body integrations [see Section 2.1 of Liu & Lai (2018) for details]. In the orbital evolution, we include the contributions from the external companion that generate LK oscillations up to the octupole level of approximation, the post-Newtonian (PN) correction due to general relativity (GR), and the dissipation due to gravitational wave (GW) emission.

The LK mechanism induces the oscillations in the eccentricity and mutual orbital inclination on the timescale

$$t_{\text{LK}} = \frac{1}{n} \frac{m_{12}}{m_3} \left(\frac{a_{\text{out,eff}}}{a} \right)^3, \quad (1)$$

where $n = (Gm_{12}/a^3)^{1/2}$ is the mean motion of the inner binary, and $a_{\text{out,eff}} \equiv a_{\text{out}} \sqrt{1 - e_{\text{out}}^2}$ is the effective outer binary separation.

During the LK oscillations, the short-range force effects (such as GR-induced apsidal precession) play a crucial role in determining the maximum eccentricity e_{max} of the inner binary (e.g., Fabrycky & Tremaine 2007). In the absence of energy dissipation, the evolution of the triple is governed by two conservation laws: the total orbital angular momentum and the total energy of the system. The analytical expression for e_{max} for general hierarchical triples (arbitrary masses and eccentricities) can be obtained in the double-averaged secular approximation if the disturbing potential is truncated to the quadrupole order. Using the method of Liu et al. (2015)

(see also Anderson et al. 2016, 2017), we find

$$\frac{3}{8} \left\{ e_0 + (j_{\min}^2 - 1) + (5 - 4j_{\min}^2) \right. \\ \times \left[1 - \frac{(j_{\min}^2 - 1)\eta_{\min} + e_0^2\eta_0 - 2j_0 \cos I_0}{4j_{\min}^2} \right]^2 \\ \left. - (1 + 4e_0^2 - 5e_0^2 \cos^2 \omega_0) \sin^2 I_0 \right\} + \varepsilon_{\text{GR}} (j_0^{-1} - j_{\min}^{-1}) = 0, \quad (2)$$

where e_0 , I_0 and ω_0 are the initial eccentricity, inclination and longitude of the periape of the inner binary, respectively, and we have defined $j_{\min} \equiv \sqrt{1 - e_{\max}^2}$, $j_0 \equiv \sqrt{1 - e_0^2}$, $\eta_{\min} \equiv L(e = e_{\max})/L_{\text{out}}$, $\eta_0 \equiv L(e = e_0)/L_{\text{out}}$ and $\varepsilon_{\text{GR}} = (3Gm_{12}^2 a_{\text{out,eff}}^3)/(c^2 a^4 m_3)$. Note that for $e_0 = 0$, Equation (2) reduces to Equation (24) of Anderson et al. (2017). For the general L/ L_{out} , the maximum possible e_{\max} for all values of I_0 , called e_{lim} , is given by (assuming $\omega_0 = 0$)

$$\frac{3}{8} \left\{ (j_{\text{lim}}^2 - 1) \left[\frac{\eta_{\min}^2}{4} \left(\frac{4}{5} j_{\text{lim}}^2 - 1 \right) - 3 \right] \right. \\ \left. + \frac{e_0^4}{(j_{\text{lim}}^2 - 1)} \frac{\eta_0^2}{4} \left(\frac{4}{5} j_{\text{lim}}^2 - 1 \right) \right. \\ \left. + 2e_0^2 \left[\frac{\eta_{\min}\eta_0}{4} \left(\frac{4}{5} j_{\text{lim}}^2 - 1 \right) + 1 \right] \right\} + \varepsilon_{\text{GR}} (j_0^{-1} - j_{\text{lim}}^{-1}) = 0, \quad (3)$$

where $j_{\text{lim}} \equiv \sqrt{1 - e_{\text{lim}}^2}$.

For systems with $m_1 \neq m_2$ and $e_{\text{out}} \neq 0$, the octupole effect may become important. The strength of the octupole effect is characterized by

$$\varepsilon_{\text{oct}} \equiv \frac{m_1 - m_2}{m_1 + m_2} \frac{a}{a_{\text{out}}} \frac{e_{\text{out}}}{1 - e_{\text{out}}^2}. \quad (4)$$

The octupole terms tend to widen the inclination window for large eccentricity excitation. However, the analytic expression for e_{lim} given by Equation (3) remains valid even when the octupole effect is strong (Liu et al. 2015; Muñoz et al. 2016; Anderson et al. 2017).

The validity of secular approximation depends on the hierarchy level of the triple system. For sufficiently hierarchical systems, the angular momenta of the inner and outer binaries exchange periodically over a long timescale (longer than the companion's orbital period), while the exchange of energy is negligible. When the eccentricity variation timescale of the inner binary is longer than the period of companion's orbit (P_{out}), i.e.,

$$t_{\text{LK}} \sqrt{1 - e_{\max}^2} \gtrsim P_{\text{out}}, \quad (5)$$

the double-averaged (DA) secular equations are valid. The full equations of motion can be found in Liu et al. (2015).

For moderately hierarchical systems, when the eccentricity evolution timescale at $e \sim e_{\max}$ lies between the inner orbital period P_{in} and the outer orbital period P_{out} ,

i.e.,

$$P_{\text{in}} \lesssim t_{\text{LK}} \sqrt{1 - e_{\max}^2} \lesssim P_{\text{out}}, \quad (6)$$

the DA secular equations break down, but the single-averaged (SA) secular equations remain valid. The explicit SA equations of motion are provided in Section 2.1.2 of Liu & Lai (2018).

If the tertiary companion is even closer, the perturbation becomes sufficient strong and Equation (6) may not be satisfied. In this situation, the dynamics can only be solved by N-body (NB) integrations. In this paper, we use a new N-body code developed by Yi-Han Wang based on the ARCHAIN algorithm (Mikkola & Merritt 2008). This algorithm employs a regularized integrator to accurately trace the motion of tight binaries with arbitrarily large mass ratios, and a chain structure to reduce the round-off errors from close encounters. The code uses the Bulirsch-Stoer (BS) integrator (e.g., Stoer 1972) and further reduces the round-off error by using active error compensation. Our developing code can be found at [SpaceHub](#).

All calculations in this paper, whether based on DA or SA secular equations, or NB integrations, include the PN effect of the inner binary (which gives rise to the apsidal advance) and the 2.5 PN effect (which accounts for gravitational radiation).

2.2. Spin-Orbit Coupling

To incorporate the spin-orbit coupling effect, we introduce the spin vector $\mathbf{S}_1 = S_1 \hat{\mathbf{S}}_1$ (where S_1 is the magnitude of the spin angular momentum of m_1 and $\hat{\mathbf{S}}_1$ is the unit vector). The de Sitter precession of $\hat{\mathbf{S}}_1$ around $\hat{\mathbf{L}}$ (1.5 PN effect) is governed by (e.g., Barker & O'Connell 1975)

$$\frac{d\hat{\mathbf{S}}_1}{dt} = \boldsymbol{\Omega}_{\text{SL}} \times \hat{\mathbf{S}}_1. \quad (7)$$

Let $\mathbf{r}_{1(2)}$ and $\mathbf{v}_{1(2)}$ be the position vector and velocity vector of the first and second body of the inner binary, respectively, and define $\mathbf{r} = \mathbf{r}_1 - \mathbf{r}_2$, $r = |\mathbf{r}|$, and $\mathbf{v} = \mathbf{v}_1 - \mathbf{v}_2$. The precession rate in Equation (7) is given by

$$\boldsymbol{\Omega}_{\text{SL}}^{\text{PN}} = G \left(2 + \frac{3m_2}{2m_1} \right) \frac{\boldsymbol{\mu} \mathbf{r} \times \mathbf{v}}{c^2 r^3}. \quad (8)$$

Averaging over the inner orbital period (P_{in}), the precession rate becomes

$$\boldsymbol{\Omega}_{\text{SL}}^{(\text{AV})} = \frac{3Gn(m_2 + \mu/3)}{2c^2 a(1 - e^2)} \hat{\mathbf{L}} = \Omega_{\text{SL}}^{(\text{AV})} \hat{\mathbf{L}}. \quad (9)$$

Similar equations apply to \mathbf{S}_2 . Note that the back-reaction torques from $\hat{\mathbf{S}}_1$ on $\hat{\mathbf{L}}$ is usually negligible since $S_1 \ll L$, and the spin-spin coupling (2 PN correction) is always negligible until the very last merging stage. Both are ignored in our calculations. In addition, the de Sitter precession of $\hat{\mathbf{S}}_1$ induced by the tertiary companion is neglected as well. Thus, the DA/SA secular equations combined with Equation (9), or N-body integration with Equation (8), completely determine the orbital and spin evolution of merging BH binaries in triples.

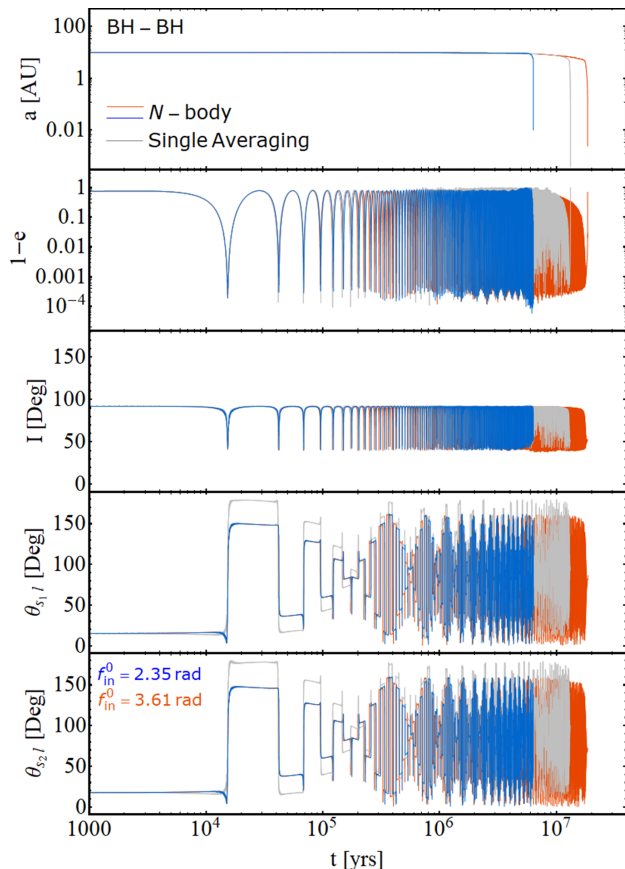


FIG. 1.— Sample orbital and spin evolution of a BH binary system with a tertiary companion. The three top panels show the semi-major axis, eccentricity and inclination (relative to $\hat{\mathbf{L}}_{\text{out}}$) of the inner BH binary, and the bottom panel show the spin-orbit misalignment angle θ_{s1} (the angle between \mathbf{S}_1 and \mathbf{L}). The system parameters are: $m_1 = 30M_\odot$, $m_2 = 20M_\odot$, $m_3 = 30M_\odot$, $a_0 = 10\text{AU}$, $a_{\text{out}} = 200\text{AU}$, $e_0 = 0.3$, $e_{\text{out}} = 0.1$, $I_0 = 91.85^\circ$, and $\theta_{s1}^0 = 15.13^\circ$, $\theta_{s2}^0 = 17.64^\circ$. The initial longitudes of periastron of the inner and outer orbits (i.e., the angle between \mathbf{e} and line of the ascending node of the two orbits) are $\omega_{\text{in},0} = 340^\circ$ and $\omega_{\text{out},0} = 113^\circ$. Different colors denote two integration methods. In our calculations, the initial true anomaly (f_{out}^0) of the outer binary is set to be π ; in the N-body calculations, the initial true anomaly (f_{in}^0) of the inner orbit is set to 2.35 rad (blue) and 3.61 rad (red).

2.3. Some Examples

To calibrate our different approaches, Figure 1 shows an example of the orbital and spin evolution of a BH binary with an inclined companion, obtained using N-body integration and SA secular equations. The parameters of the system (given in the figure caption) satisfy the SA criterion (Equation 6). We see that the SA equations succeed in resolving the “correct” orbital evolution, producing the same period and amplitude of LK cycles as in the N-body calculations. However, in the N-body calculations, the long term evolution of the binary depends on the initial true anomaly f_{in}^0 of the inner orbit, with the merger time depending on f_{in}^0 . The evolution based on the SA equation yields an “averaged” merger time. Note that in this example, the “residual” eccentricity (i.e., the binary eccentricity when it enters the LIGO band) is neg-

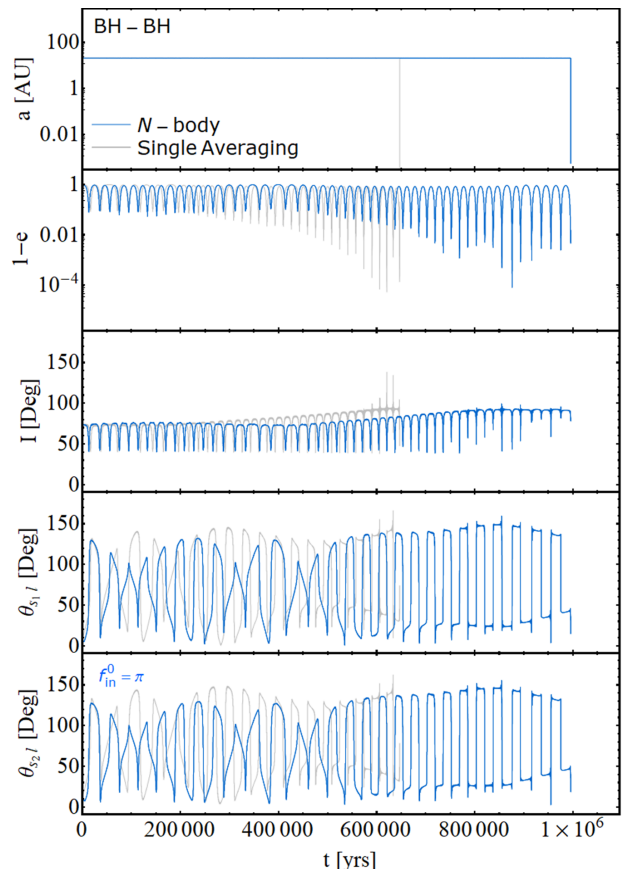


FIG. 2.— Another example of the orbital and spin evolution of a BH binary in triple system. The system parameters are: $m_1 = 30M_\odot$, $m_2 = 20M_\odot$, $m_3 = 49.78M_\odot$, $a_0 = 20.80\text{AU}$, $a_{\text{out}} = 381.39\text{AU}$, $e_0 = 0.017$, $e_{\text{out}} = 0.699$, $I_0 = 73.60^\circ$, $\omega_{\text{in},0} = 111.39^\circ$, $\omega_{\text{out},0} = 234.54^\circ$, and $\theta_{s1}^0 = 7.9^\circ$, $\theta_{s2}^0 = 12.5^\circ$. In this example, the initial true anomalies of the inner and outer binaries are set to π .

ligible ($e_m \ll 1$) regardless of the integration methods.

The bottom panel of Figure 1 shows that the spin axis $\hat{\mathbf{S}}_1$ (initially misaligned with respect to $\hat{\mathbf{L}}$ by 15°) experiences large variations during the inner binary evolution. As discussed in Liu & Lai (2018), a useful “adiabaticity parameter” characterizing the spin evolution is (see also Storch et al. 2014; Storch & Lai 2015; Anderson et al. 2016, 2017)

$$\mathcal{A} \equiv \left| \frac{\Omega_{\text{SL}}^{(\text{AV})}}{\Omega_{\text{L}}} \right|, \quad \text{with} \quad \Omega_{\text{L}} = \frac{3(1+4e^2)|\sin 2I|}{8t_{\text{LK}}\sqrt{1-e^2}}. \quad (10)$$

As the orbit decays, the spin dynamics transitions from the “weak coupling” regime ($\mathcal{A} \ll 1$) to the “strong coupling” regime ($\mathcal{A} \gg 1$). The spin-orbit misalignment angle tends to be frozen at a high value near the end of the inspiral. In this example, all integrations produce large final spin-orbit misalignment angles, $\theta_{s1}^f \simeq 81^\circ$, $\theta_{s2}^f \simeq 77^\circ$ ($f_{\text{in}}^0 = 2.35$ rad) and $\theta_{s1}^f \simeq 87^\circ$, $\theta_{s2}^f \simeq 72^\circ$ ($f_{\text{in}}^0 = 3.61$ rad) for the N-body integration, and $\theta_{s1}^f \simeq \theta_{s2}^f \simeq 90^\circ$ for the SA secular integration.

Figure 2 depicts another example of BH binary merger, in which the octupole effect is important. The system

parameters (given in the figure caption) imply that both DA and SA approaches are not accurate. We see that in the N-body integration, due to the high-efficiency of gravitational radiation at e_{\max} , rapid merger occurs, accompanied by highly eccentric orbit ($e_m \simeq 0.94$) when the GW frequency enters the LIGO band. Because of the rapid orbital decay, the spin vector does not experience large variation and the final spin-orbit misalignment angle freezes at $\theta_{s1}^f \simeq 15^\circ$, $\theta_{s2}^f \simeq 18^\circ$. However, for the SA secular integration, the residual eccentricity is “erased” ($e_m \simeq 0.05$) and the final spin-orbit misalignment angle are $\theta_{s1}^f \simeq 39^\circ$, $\theta_{s2}^f \simeq 22^\circ$.

3. POPULATION STUDY

3.1. Parameter Choice and System Setup

We consider two types of merging binaries in this paper. The first has masses $(m_1, m_2) = (30M_\odot, 20M_\odot)$, representing typical BH-BH binaries; the second has $(m_1, m_2) = (30M_\odot, 1.4M_\odot)$, representing BH-NS binaries. For each inner binary, we consider all possible initial binary/triple systems and parameters that may lead to binary mergers. In particular, the initial semimajor axes of the inner and outer orbits (a_0 and a_{out}) are chosen from a log-uniform distribution from 10 AU to 10^4 AU; the initial orbital eccentricities are drawn from a uniform distribution ranging from 0 to 1 for both inner and outer binary orbits; the tertiary companion mass is assigned by assuming a flat distribution in $(0, 1)$ for m_3/m_{12} (e.g., Sana et al. 2012; Duchêne & Kraus 2013; Kobulnicky et al. 2014); the binary inclinations are isotropically distributed (uniform distribution in $\cos I_0$). Since the velocity kick during the BH formation may introduce small spin-orbit misalignment, we consider a flat distribution of the initial $\cos \theta_{\text{sl}}^0$ in the range $(\cos 0^\circ, \cos 20^\circ)$.

For the triple systems to be dynamically stable, the ratio of the pericenter distance of the outer orbit to the apocenter distance of the inner orbit must satisfy (e.g., Kiseleva et al. 1996)

$$\frac{a_{\text{out}}(1 - e_{\text{out}})}{a(1 + e)} > \frac{3.7}{Q_{\text{out}}} - \frac{2.2}{1 + Q_{\text{out}}} + \frac{1.4}{Q_{\text{in}}} \frac{Q_{\text{out}} - 1}{Q_{\text{out}} + 1}, \quad (11)$$

where $Q_{\text{in}} = [\max(m_1, m_2)/\min(m_1, m_2)]^{1/3}$ and $Q_{\text{out}} = (m_{12}/m_3)^{1/3}$.

For each type of binaries, simulations are performed for 10^5 randomly chosen initial conditions. After extracting the stable triples based on Equation (11), we identify the parameter regime for each triple according to the criteria of Section 2.1. We use $e_{\max} = e_{\text{lim}}$ in Equations (5) and (6). Different integration methods (DA/SA/NB) are then applied to systems in different regimes. This helps us to speed up our calculations and ensures the accuracy of system evolution.

To further increase the efficiency of the parameter survey, we adopt the following “stopping conditions”. First, the maximum integration time is set to be the minimum of $(10^4 t_{\text{LK}}, 10 \text{ Gyrs})$. This maximum time is adequate to capture the most of the mergers. Moreover, we terminate

the simulation when the inner binary semimajor axis is reduced to less than 0.5% of the initial a_0 and when the adiabaticity parameter $\mathcal{A} \gg 1$. This is reasonable because in the last phase of the binary merger, the binary dynamics is dominated by GW emission such that the inner binary is decoupled from the perturbation of the tertiary companion. The condition $\mathcal{A} \gg 1$ ensures that the spin-orbit misalignment angle θ_{sl} reaches its “final” (constant) value. Once the full integration is stopped, the subsequent evolution of the inner binary eccentricity and semimajor axis can be obtained using the analytical formulas of Peters (1964). This allows us to obtain the residual eccentricity e_m when binary enters LIGO detection band, i.e., when the peak GW frequency (Wen 2003)

$$f_{\text{GW}}^{\text{peak}} = \frac{(1 + e)^{1.1954}}{\pi} \sqrt{\frac{G(m_1 + m_2)}{a^3(1 - e^2)^3}} \quad (12)$$

reaches 10 Hz.

3.2. Parameter Space for Binary Mergers

What kinds of triple systems can produce binary mergers? For our canonical BH-BH binaries ($m_1 = 30M_\odot, m_2 = 20M_\odot$), we find 1092 mergers out of 25255 stable systems, with merger fraction 4.3%; this includes 114 mergers out of 10243 systems in DA parameter regime (fraction $\simeq 1.1\%$), 373 mergers out of 5785 systems in SA parameter regime (fraction $\simeq 6.5\%$), and 605 mergers out of 9277 systems from direct NB simulations (fraction $\simeq 6.6\%$). Figure 3 depicts the parameter space that produces BH mergers, where we plot the initial binary separation ratio a_{out}/a_0 and $\bar{a}_{\text{out,eff}}/a_0$ versus the inclination (I_0) between the inner and outer orbits. We also plot the distribution of I_0 in the top panel. Here, we introduce the dimensionless scaled semi-major axis

$$\bar{a}_{\text{out,eff}} \equiv \left(\frac{a_{\text{out}} \sqrt{1 - e_{\text{out}}^2}}{1 \text{ AU}} \right) \left(\frac{m_3}{1 M_\odot} \right)^{-1/3} \quad (13)$$

to characterize the “strength” of the tertiary companion. The final outcome of each integration is also indicated by the color (quick, moderate and slow mergers, corresponding to merger time $T_m \leq 10^6 \text{ yrs}$, $10^6 \text{ yrs} < T_m \leq 10^8 \text{ yrs}$ and $T_m > 10^8 \text{ yrs}$, respectively) and by the symbol (DA, SA and NB integration methods).

As shown in Figure 3, there is a preference for initially highly inclined systems (around $I_0 \sim 90^\circ$) to generate mergers. This is the typical outcome for “quadrupole” systems, for which the two members of the inner binary have comparable masses such that $\varepsilon_{\text{oct}} \ll 1$ (see Equation 4). The distribution shows that mergers occur at a wide range of initial inclinations, but the number decreases sharply when I_0 goes below 40° or above 140° . Therefore, we do not simulate the triples outside this “Kozai window”. From the middle and bottom panels, we see that the quick and slow mergers have no obvious trend in a_{out}/a_0 and $\bar{a}_{\text{out,eff}}/a_0$. However, the majority of mergers happen with $a_{\text{out}}/a_0 \lesssim 100$ and $\bar{a}_{\text{out,eff}}/a_0 \lesssim 20$.

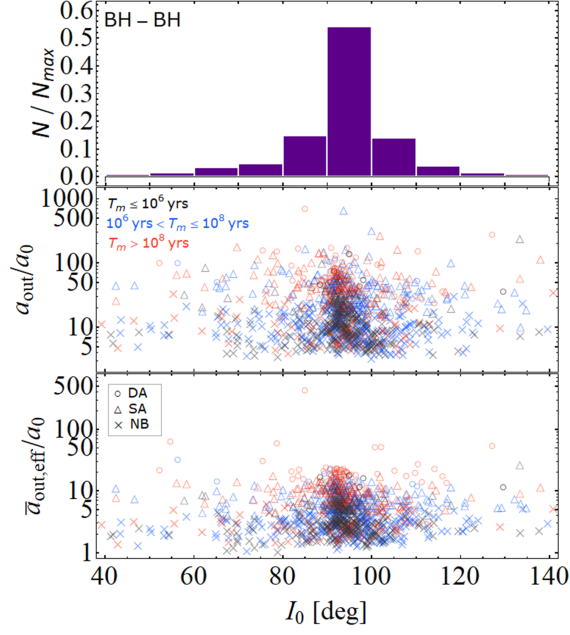


FIG. 3.— Parameter space producing BH mergers in triple systems (with $m_1 = 30M_\odot, m_2 = 20M_\odot$). Top panel: the distribution of initial inclination between the inner and outer orbits. Middle panel: initial binary separation ratio a_{out}/a_0 versus I_0 . Bottom panel: ratio between the scaled outer semimajor axis (Equation 13) and the inner one $\bar{a}_{\text{out,eff}}/a_0$. Results are separated into three ranges of merger time (colors) and three integration methods (symbols), as labeled: double-averaged (DA), single-averaged (SA) secular equations and N-body (NB) calculation, which are relevant to different parameter regimes (see Equations 5-6).

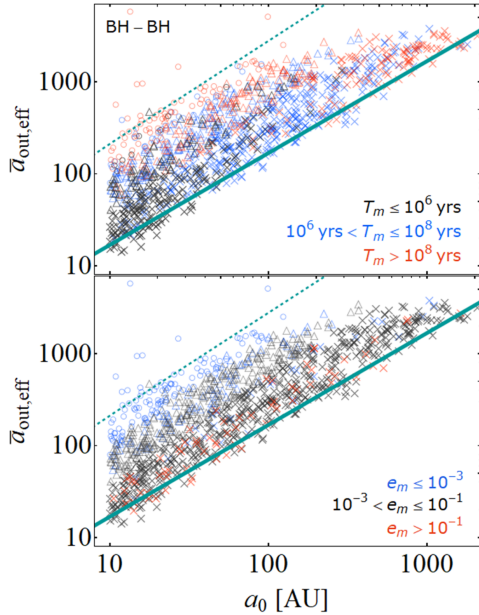


FIG. 4.— Parameter space producing BH-BH mergers presented in Figure 3. Different merger times and residual eccentricities are color coded as labeled in the upper and lower panels, respectively. The three types of symbols indicate the mergers achieved by DA, SA and NB integrations (same as Figure 3). The solid lines represent the stability criterion (Equation 11 with $e_0 = 1, e_{\text{out}} = 0$ and $m_3 = m_{12} = 50M_\odot$). The dashed lines represent the requirement for the detectable mergers in LK channel (Equation 14 with e_m given by Equation 3 using $e_0 = 0$ and $\eta_0 = 0$).

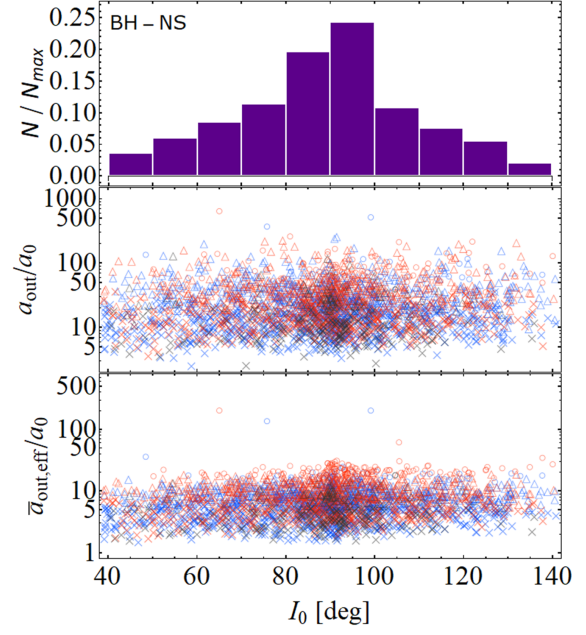


FIG. 5.— Same as Figure 3, but for our canonical BH-NS binaries (with $m_1 = 30M_\odot, m_2 = 1.4M_\odot$).

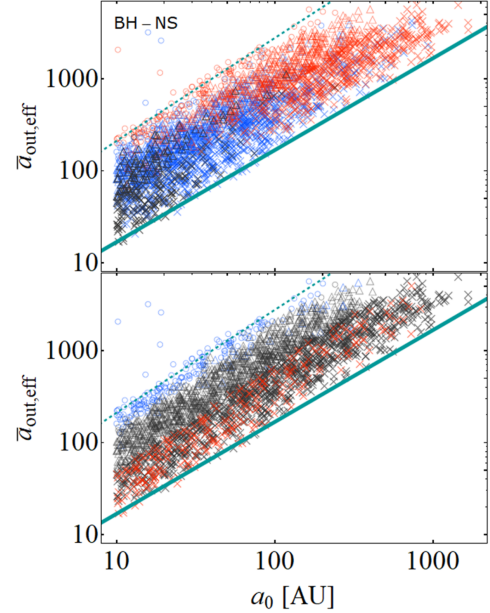


FIG. 6.— Same as Figure 4, but for our canonical BH-NS binaries.

In Figure 4, we plot the initial conditions in terms of $(\bar{a}_{\text{out,eff}}, a_0)$ for BH mergers presented in Figure 3. The upper and lower panels show the outcomes indicated by different merger times and “residual” eccentricities (i.e., the binary eccentricity when the peak GW frequency enters the LIGO band). The solid line comes from the stability criterion (Equation 11), set by $e_0 = 1, e_{\text{out}} = 0$ and $m_3 = m_{12} = 50M_\odot$. The dashed line is obtained by the condition

$$T_{\text{m},0}(1 - e_{\text{max}}^2)^3 = 10^{10} \text{ yrs}, \quad (14)$$

where $T_{\text{m},0} \equiv (5c^5 a_0^4)/(256G^3 m_{12}^2 \mu)$ is the merger time

due to GW radiation of an isolated binary with the initial semi-major axis a_0 and eccentricity $e_0 = 0$, and e_{\max} is evaluated by Equation (3) at $e_0 = 0$ and $\eta_0 \rightarrow 0$. In Equation (14), the left-hand side represents the merger time of the inner binary when its eccentricity is excited to e_{\max} during a LK cycle (Liu & Lai 2018; Randall & Xianyu 2018)¹. Thus, Equation (14) provides the upper limit of merger time for detectable LK-induced mergers.

In the upper panel of Figure 4, we see that the quick BH mergers ($T_m \lesssim 10^6$ yrs) are likely to occur when both $\bar{a}_{\text{out,eff}}$ and a_0 are relatively small. In the lower panel, the eccentric mergers ($e_m \gtrsim 0.1$) preferentially arise for combinations of $(\bar{a}_{\text{out,eff}}, a_0)$ that are located near the stability boundary. This implies that the highest eccentricity excitations require the strongest perturbers.

For our canonical BH-NS binaries (with $m_1 = 30M_\odot$, $m_2 = 1.4M_\odot$), the octupole effect becomes important due to the high mass ratio. Previous works (Liu et al. 2015; Anderson et al. 2017) have shown that the main effect of the octupole potential is to broaden the range of the initial I_0 for extreme eccentricity excitations ($e_{\max} = e_{\text{lim}}$). In our simulations, we find 2683 mergers out of 26238 stable triple systems, with a merger fraction of 10.2%; this includes 209 mergers out of 9761 systems in DA regime (fraction $\simeq 2.14\%$), 1197 mergers out of 6010 systems in SA regime (fraction $\simeq 20\%$) and 1277 out of 10467 systems in direct NB simulations (fraction $\simeq 12\%$). The somewhat smaller merger fraction in the NB regime compared to the SA regime arises because some systems become dynamically unstable during the NB integrations.

Figure 5 shows the dependence on the initial parameters for BH-NS merger events. Compared to Figure 3 we see that a large range of the initial inclinations inside the Kozai window produces mergers, as a result of the non-negligible ϵ_{oct} for BH-NS systems.

Figure 6 shows the similar result as Figure 4, but for BH-NS binaries. Since the merger fraction is much larger than the BH-BH case, the statistical features (parameter spaces) for producing quick or eccentric mergers become more evident.

3.3. Merger Properties

In Figure 7, we show the distributions of the merger time T_m , merger eccentricity e_m and spin-orbit misalignment angle θ_{sl}^f for our canonical BH-BH mergers. As shown in the top left panel, most merger events occur around $T_m \sim 10^{7-8}$ yrs. We find that about 80% of the binaries enter the LIGO band with $e_m \gtrsim 10^{-3}$, 50% have $e_m \gtrsim 10^{-2}$, 7% have $e_m > 0.1$, and 0.7% have $e_m > 0.9$ (see the top right panel). In the lower panels, we see that there is a slight clustering around 90° for the final spin-orbit misalignment θ_{sl}^f . This 90° ‘‘attractor’’ arise from quadruple-dominated mergers [corresponding to CASE I discussed in Section 4.2 in Liu & Lai (2018)]. The other

¹ Note that this expression is valid only for systems in the DA regime and with $\epsilon_{\text{oct}} \ll 1$ and $1 - e_{\max} \ll 1$; see Liu & Lai (2017, 2018)

peak around $\theta_{\text{sl}}^f = 0^\circ$ is associated with CASE III and IV [see Liu & Lai (2018) for details].

Figure 8 shows the results for our canonical BH-NS binaries. Because of the low NS mass, the orbital decay due to GW is not as efficient as the BH-BH case. As seen in the upper left panel, there is only a few merger events with $T_m < 10^5$ yrs. Compared to the BH-BH case, the high mass ratio of BH-NS binaries leads to stronger octupole effect, which enhances extreme eccentricity excitation. In the upper right panel, we see a significant increase in the number of mergers with appreciable e_m : Out of all merger events, about 93% have $e_m \gtrsim 10^{-3}$, 80% have $e_m \gtrsim 10^{-2}$, 18% have $e_m > 0.1$, and 2.5% have $e_m > 0.9$. The octupole effect may also produce chaotic orbital evolution (e.g., Lithwick & Naoz 2011; Li et al. 2014; Liu et al. 2015), such that the spin-orbit misalignment angle is allowed to settle to any value (CASE II in Liu & Lai 2018). Thus, we find in the lower panels of Figure 8 that the final spin-orbit misalignments are largely isotropic (i.e., uniform in $\cos \theta_{\text{sl}}^f$).

To determine how the final spin-orbit misalignment θ_{sl}^f depends on the initial θ_{sl}^0 , Figure 9 shows the distribution of θ_{sl}^f for different ranges of initial θ_{sl}^0 ($0^\circ - 10^\circ$ versus $10^\circ - 20^\circ$). We see that for BH-BH mergers, the peak around $\theta_{\text{sl}}^f = 90^\circ$ exist regardless of the initial range of θ_{sl}^0 . For BH-NS mergers, the distribution of $\cos \theta_{\text{sl}}^f$ is approximately uniformly for different ranges of θ_{sl}^0 .

Several previous works also studied eccentric mergers of BH binaries induced by a tertiary companion (Antonini et al. 2017) (see also Rodriguez & Antonini 2018) combined stellar evolution (mass loss and natal kick) and dynamics in isolated triples, and found that about 10% of BH mergers have $e_m > 0.1$, similar to our result. On the other hand, Silsbee & Tremaine (2017) also considered stellar evolution and used N-body integration to evolve the triples, and found that a few percent of the mergers may have $e_m > 0.999$ (In contrast we found about 1% having $e_m \gtrsim 0.9$). In the case of BH mergers induced by a massive BH, Antonini & Perets (2012) claimed that 10% have $e_m > 0.1$ (see also Fragione & Bromberg 2019). In dense star clusters, about 1% of the BH mergers generated by scattering processes may have $e_m > 0.1$ (e.g., Samsing & Ramirez-Ruiz 2017; Rodriguez et al. 2018). Thus, despite the uncertainties in various scenarios, the detection of eccentric BH mergers would constrain the dynamical formation channels of binary BHs.

3.4. χ_{eff} and Correlation with Merger Eccentricity e_m

Having obtained the distributions of $\cos \theta_{\text{s}1}^f$ and $\cos \theta_{\text{s}2}^f$ in Section 3.3, we can calculate the distribution of the effective spin parameter

$$\chi_{\text{eff}} = \frac{m_1 \chi_1 \cos \theta_{\text{s}1}^f + m_2 \chi_2 \cos \theta_{\text{s}2}^f}{m_{12}}, \quad (15)$$

where $\chi_{1,2} \leq 1$ are the Kerr parameters. Figure 10 (lower panel) shows three examples with different $\chi_{1,2}$. Here, $\chi_{\text{eff}}^{\text{max}} = (m_1 \chi_1 + m_2 \chi_2) / m_{12}$ is the maximum possible value of χ_{eff} for given $m_1 \chi_1$ and $m_2 \chi_2$ (this maximum is

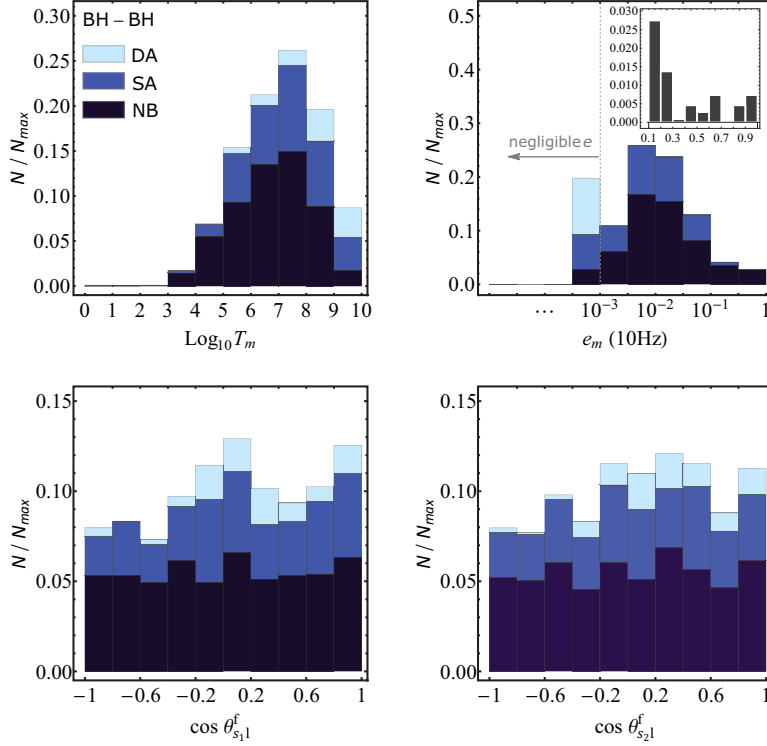


FIG. 7.— Distributions of the merger time T_m , eccentricity e_m (when the binary enters the LIGO band at 10 Hz), and spin-orbit misalignment angle for BH-BH mergers in triples (see Figure 3). The results are for systems in different regimes, corresponding to different integration methods (DA, SA and NB). All the data is normalized by the total number of mergers, $N_{\max} = 1092$, including 114 (DA), 373 (SA) and 605 (NB) mergers out of 25255 simulated systems. In the top right panel, we group all the $e_m < 10^{-3}$ mergers together and show the zoom-in version of the mergers with $e_m > 0.1$.

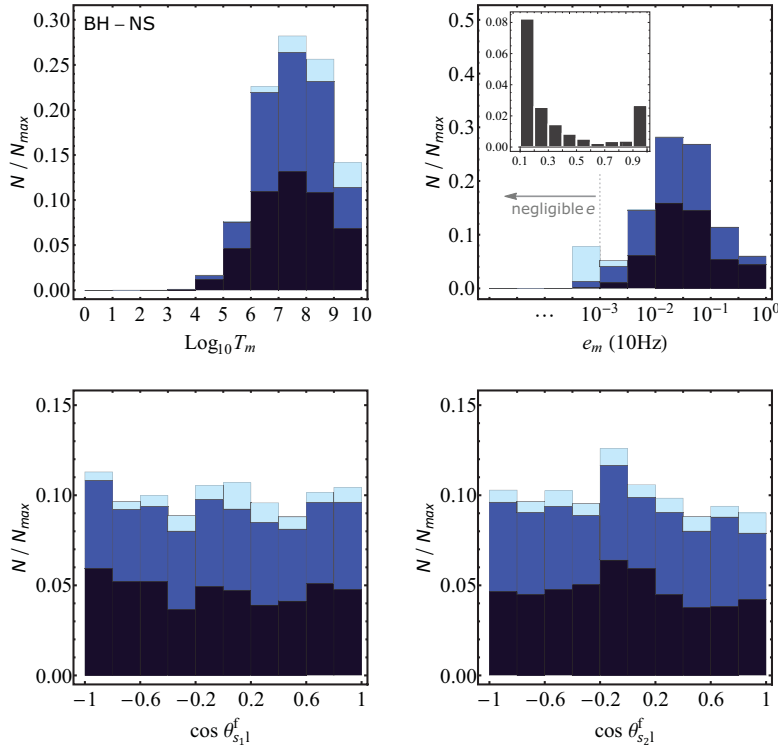


FIG. 8.— Same as Figure 7, except for BH-NS binaries (see Figure 5). The data represents $N_{\max} = 2683$ mergers, including 209 (DA), 1197 (SA) and 1277 (NB) mergers out of 26238 simulated systems.

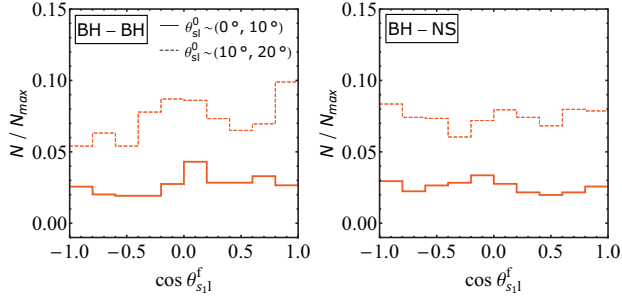


FIG. 9.— Distribution of the final spin-orbit misalignment θ_{s1}^f for BH-BH mergers and BH-NS mergers in triples. We separate the mergers with different ranges of initial spin-orbit orientations, i.e., $\theta_{sl}^0 \in (0^\circ, 10^\circ)$ and $\theta_{sl}^0 \in (10^\circ, 20^\circ)$.

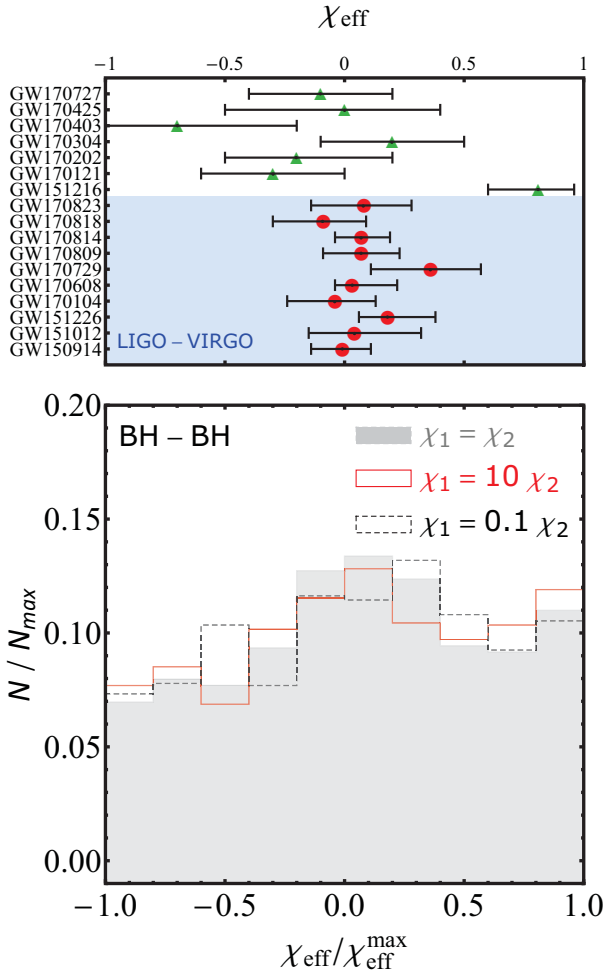


FIG. 10.— Upper panel: All the public detection of BH-BH mergers (as of April 2019), reported by Abbott et al. (2018a) (red circle) and Zackay et al. (2019); Venumadhav et al. (2019) (green triangle). Lower panel: The distribution of the rescaled binary spin parameter χ_{eff} [Equations 15; and $\chi_{\text{eff}}^{\text{max}} = (m_1\chi_1 + m_2\chi_2)/m_{12}$] for the merging BH-BH binaries depicted in Figure 7.

achieved at $\cos\theta_{s1}^f = \cos\theta_{s2}^f = 1$). The different ratios of χ_1 and χ_2 affect the distribution of $\chi_{\text{eff}}/\chi_{\text{eff}}^{\text{max}}$, but not significantly. The peak around $\chi_{\text{eff}} \simeq 0$ is clearly visible, although not as distinct as in Liu & Lai (2018), who considered a more limited parameter space. The full range

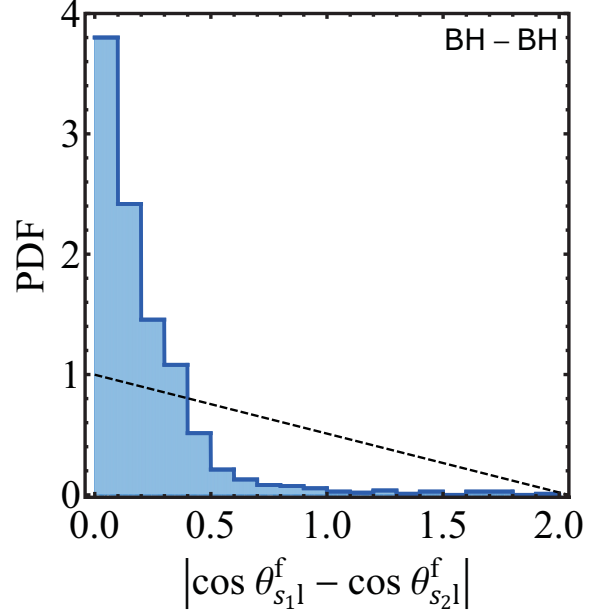


FIG. 11.— The distribution of $|\cos\theta_{s1}^f - \cos\theta_{s2}^f|$ for merging BH-BH binaries, where the data comes from Figure 7. The dashed line represents Equation (17), obtained assuming uncorrelated isotropic spin distributions.

of χ_{eff} values (from negative to positive) becomes possible. This is in contrast to the isolated stellar binary evolution channel, which always predict positive χ_{eff} because of the preferentially aligned spins after the binaries undergo mass transfer or tidal coupling (e.g., Zaldarriaga et al. 2017; Gerosa et al. 2018). Comparison with current LIGO/VIRGO detections (top panel of Figure 10) suggests that the triple-driven merger scenario may be required, but obviously it is premature to draw any firm conclusion at this point, because of the (partial) degeneracy between χ_1 , χ_2 and spin-orbit misalignment angles.

For BH-NS binaries, $\chi_{\text{eff}} \simeq \chi_1 \cos\theta_{s1}^f$, and the peak around $\chi_{\text{eff}} \simeq 0$ is insignificant because of the random distribution of the final spin-orbit misalignment angles (see Figure 8).

If the distributions of $\cos\theta_{s1}^f$ and $\cos\theta_{s2}^f$ are uncorrelated, as we may expect to be the case for $m_1 \neq m_2$, when the octupole effect is significant, the distribution of $|\cos\theta_{s1}^f - \cos\theta_{s2}^f|$ can be derived directly, where $\mu_1 \equiv \cos\theta_{s1}^f$ and $\mu_2 \equiv \cos\theta_{s2}^f$. Given $P_1(\mu_1)$ and $P_2(\mu_2)$, the distribution function of $\Delta\mu$ is

$$P(\Delta\mu) = \int_{-1}^{1-\Delta\mu} P_1(\mu_1)d\mu_1 \int_{-1}^{1-\Delta\mu} P_2(\mu_2)d\mu_2 \times \delta(\Delta\mu - \mu_1 + \mu_2). \quad (16)$$

In the case where μ_1 and μ_2 are uniformly distributed, we have $P_1 = P_2 = 1/2$, and Equation (16) gives

$$P(\Delta\mu) = \begin{cases} (1/2) - (1/4)\Delta\mu, & \Delta\mu > 0, \\ (1/2) + (1/4)\Delta\mu, & \Delta\mu < 0. \end{cases} \quad (17)$$

Figure 11 shows the distribution of $|\cos\theta_{s1}^f - \cos\theta_{s2}^f|$ from the simulation data depicted in Figure 7. Compared

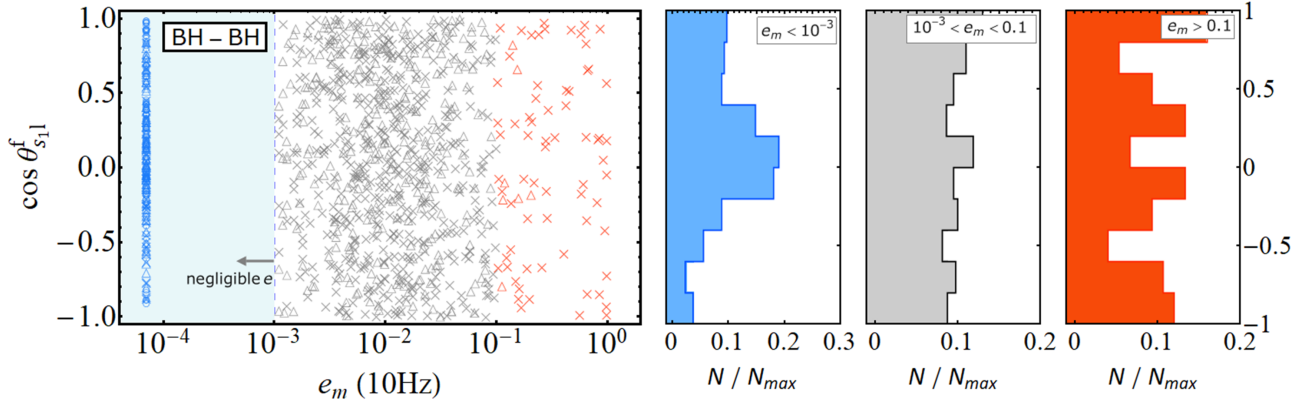


FIG. 12.— Spin-orbit misalignment distribution for BH-BH systems with different merger eccentricities. The left panel shows the final spin-orbit misalignment angles and merger eccentricities of all BH-BH merger events in our simulations. The color-coded symbols represent systems with different ranges of e_m (systems with $e_m < 10^{-3}$ are grouped together), where the symbols indicate the mergers achieved by DA, SA and NB integrations (same as Figure 3). The right three panels show the distributions of $\cos \theta_{s1}^f$ for mergers with different ranges of e_m .

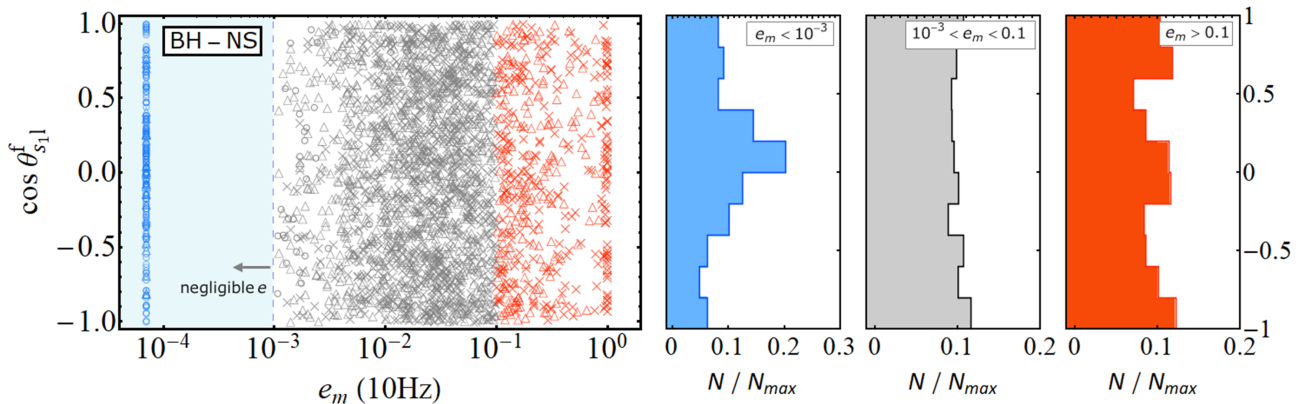


FIG. 13.— Same as Figure 12, but for BH-NS binaries.

to Equation (17), we see that the actual distribution is much more peaked around $\Delta\mu = 0$. This suggests that the two spins in the merging BH binary are correlated. Namely, in the majority of mergers, the two BHs are likely to have similar final θ_{s1}^f , although each θ_{s1}^f could be any value running from 0° to 180° .

Our previous work (Liu & Lai 2018) and those by Antonini et al. (2018) and Rodriguez & Antonini (2018) found a distinct peak in the χ_{eff} distribution around $\chi_{\text{eff}} = 0$ for sufficiently hierarchical systems. In this study, we have considered all possible stable triples covering a wide levels of hierarchy. From Figure 7, we see that highly hierarchical systems only contribute a small fraction of mergers, i.e. the majority of merging BH binaries are produced by the moderately hierarchical systems with strong tertiary companions. The resultant large number of “isotropic” final spin-orbit misalignment angles tend to “bury” the 90° signature. Thus, the $\chi_{\text{eff}} = 0$ peak in the overall distribution shown in Figure 10 is less distinct than the one found in Liu & Lai (2018) and Antonini et al. (2018).

Figure 12 illustrates the correlation between the final spin-orbit misalignment angles and merger eccentricities of BH-BH binaries. We see that the systems with $e_m \lesssim$

10^{-3} exhibit a peak around $\cos \theta_{s1}^f \simeq 0$, while those with larger e_m exhibit more uniform distribution in $\cos \theta_{s1}^f$. This is consistent with the 90° “attractor” found in Liu & Lai (2018) (CASE I in that paper), where we used DA secular equations to evolve the triple systems and spins. In that work, no significant e_m was generated for the systems considered.

In Figure 13, we consider BH-NS binaries. As in the BH-BH case (Figure 12), systems with $e_m \ll 1$ exhibit a 90° peak in the θ_{s1}^f distribution, while those with large e_m do not.

In reality, triple systems (especially the outer orbit) can be perturbed (even disrupted) by close fly-bys with other objects (e.g., Michaely & Perets 2019). The lifetime of a triple may be significantly shortened than 10^{10} years, depending on the stellar density of the surroundings. To examine mergers before the disruption of triples, we separate the mergers by the merger time ($T_m \leq 10^6 \text{ yrs}$, $10^6 \text{ yrs} < T_m \leq 10^8 \text{ yrs}$ and $T_m > 10^8 \text{ yrs}$). Figures 14 and 15 show that fast mergers (with shorter T_m) tend to have a higher probability to be accompanied by eccentric orbits at 10 Hz (i.e., $e_m > 0.1$). This is more evident for BH-NS binaries (Figure 15), where the octupole terms contribute to a large set of systems with

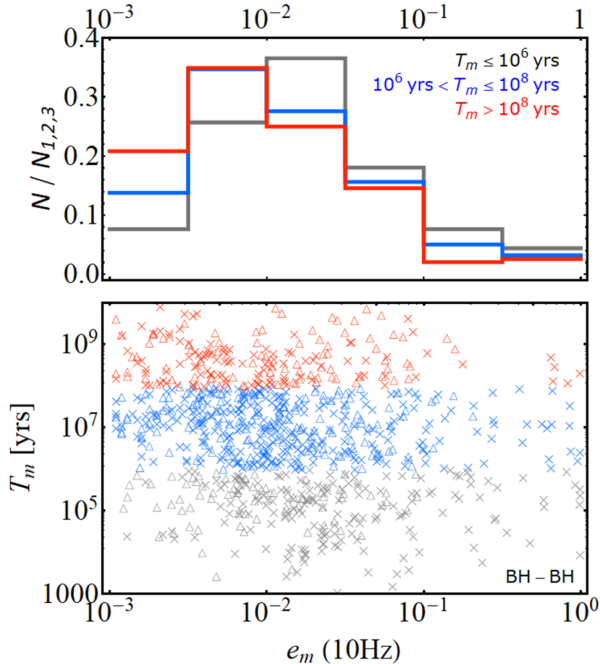


FIG. 14.— Upper panel: the distribution of the residual eccentricity for BH-BH mergers with different range of merger times (color-coded), normalized by the number of mergers in each category of T_m . Lower panel: the correlation between the merger time and residual eccentricity for each merger. The symbols indicate the mergers achieved by DA, SA and NB integrations (same as Figure 3).

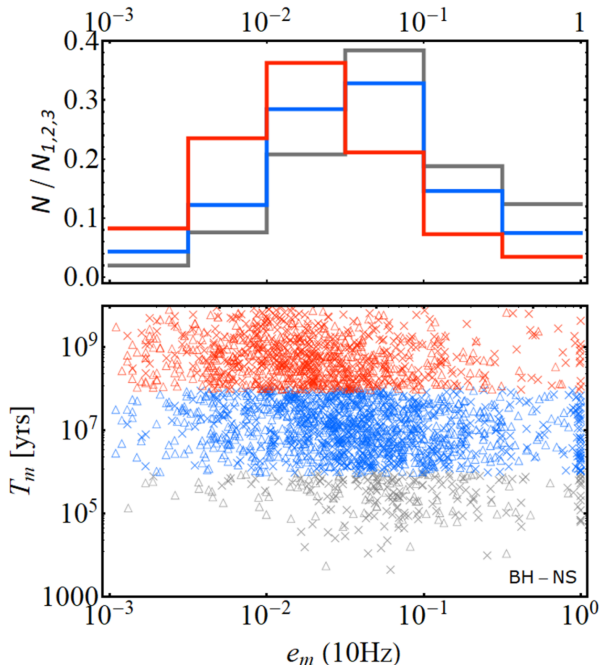


FIG. 15.— Same as Figure 14, but for BH-NS binaries.

high- e excitation and shorter merger time.

4. SUMMARY AND DISCUSSION

4.1. Summary of Key Results

In this paper, we have systematically studied the dynamical signatures of BH-BH and BH-NS mergers induced by tertiary companions in triple systems, emphasizing the detectable merger eccentricities and spin-orbit misalignments when the inner binary enters the LIGO sensitivity band (> 10 Hz). Going beyond our previous works (Liu & Lai 2017, 2018), we examined a wide range of triple systems to explore the dependence of the merger properties on the binary/triple parameters. More specifically, for two types of binaries, with $(m_1, m_2) = (30M_\odot, 20M_\odot)$ (representing a canonical BH-BH binary) and $(30M_\odot, 1.4M_\odot)$ (representing a canonical BH-NS binary), we considered all possible binary/triple configurations and parameters that lead to binary mergers and determined the distributions of merger times, eccentricities and spin-orbit misalignments. We used both single-averaged and double-averaged secular equations that include octupole terms and spin-orbit coupling (already presented in Liu & Lai 2018), as well as a newly developed N-body code based on ARCHAIN algorithm, to evolve systems with various degrees of hierarchy. This allowed us to efficiently cover a wide range of parameter space and to determine the merger properties reliably.

We first explored what kind of initial triples can produce BH-BH and BH-NS mergers within 10^{10} years. In addition to significant tertiary inclinations (as required for the Lidov-Kozai effect to be efficient), tertiary-induced mergers also require that the initial tertiary-binary separation ratio lie in the range $5 \lesssim a_{\text{out}}/a_0 \lesssim 100$, or more generally, the ratio between the scaled outer semimajor axis to the inner one, $\bar{a}_{\text{out,eff}}/a_0$ (see Eq. 13), ranges from 1 to 20 (see Figs. 3 and 5). The stability criterion of the triple and an analytical “limiting” merger time expression (Eq. 14) provide an excellent characterization of the parameter space leading to mergers (see Figs. 4 and 6).

Our studies have revealed several distinct dynamical signatures of the tertiary-driven binary merger scenario. For merging binaries with comparable masses (i.e., BH-BH binaries), we found that about 7% of the mergers have eccentricities $e_m > 0.1$ at 10 Hz, and 0.7% have $e_m > 0.9$. Distant tertiary companions (with negligible octupole effects; see Eq. 4) tend to generate spin-orbit misalignments θ_{sl}^f around 90° and negligible e_m (see Figs. 7 and 12). Closer tertiary companions (with stronger octupole effects) produce a more isotropic distribution of θ_{sl}^f and non-negligible e_m . Note that the misalignment angles θ_{sl}^f of the two BHs are correlated (see Fig. 11). We have also computed the distribution of the mass-weighted spin parameter χ_{eff} (Eq. 15) of merging BH binaries in triples. Although χ_{eff} can have a wide range of values, there still exists a characteristic shape with peak around $\chi_{\text{eff}} \simeq 0$ in its distribution (see Fig. 10). This could serve as an indicator of tertiary-induced binary mergers.

For merging binaries with high mass ratio (e.g., BH-NS binaries), we found a large fraction of systems with significant merger eccentricities as a result of the strong octupole effects: About 18% have $e_m > 0.1$ and 2.5%

have $e_m > 0.9$. Thus, the residual eccentricity at 10 Hz could indeed serve as an indicator for such tertiary-driven binary mergers. On the other hand, we found that the final spin-orbit misalignments have an approximately isotropic distribution (with an insignificant 90° peak), except for the weak octupole systems that generate mergers with negligible residual eccentricities (see Figs. 8 and 13).

Overall, our study showed that a combination of detections of e_m and θ_{sl}^f (or χ_{eff}) from future LIGO/VIRGO observations would provide key information to determine or constrain the formation channels of merging BH-BH and BH-NS binaries.

4.2. Discussion

Although in this paper we have focused on two types of binaries with specific masses – these masses can be measured from LIGO/VIRGO observations, our survey of parameter space for the initial binaries/triples was extensive. The statistical properties of tertiary-driven mergers found in this paper can be extended to other merging binaries with various mass ratios.

We have found that a small fraction of merging binaries in triples enter the LIGO band with appreciable eccentricities (7% of BH-BH binaries and 18% of BH-NS binaries have $e_m > 0.1$). However, almost all such binaries pass through the LISA band with high eccentricities (see also Samsing & D’Orazio 2018; Kremer et al. 2019; Fang et al. 2019; Randall & Xianyu 2019; Hoang et al. 2019). Thus, joint observations by LIGO/VIRGO and LISA, where the information on the BH spin and eccen-

tricity could be extracted, will be very useful to constrain the formation mechanisms of merging binaries, especially for the tertiary-driven scenario.

We have focused on triple systems in this paper. For quadrupole system, binary-binary interactions can significantly enhance the binary merger fraction (e.g., Hamers & Lai 2017; Fang et al. 2018; Hamers 2018; Liu & Lai 2019; Fragione & Kocsis 2019). Although the occurrence rate of stellar quadruples is smaller than that of stellar triples, dynamically induced BH mergers in quadruple systems may be an important channel of producing BH mergers (Liu & Lai 2019). A systematic study of the dynamical signatures of this channel is beyond the scope of this paper, although we expect that many similar features found here may carry over. As shown in Liu & Lai (2019), if the parameters of a quadruple system satisfies certain resonance criterion, the inner binary eccentricity can be driven close to unity in a chaotic way, leading to a similar behavior for θ_{sl}^f and e_m as in the cases of triples with strong octupole effects (i.e., random $\cos \theta_{\text{sl}}^f$ distribution and large e_m).

5. ACKNOWLEDGMENTS

We thank Bonan Pu for useful discussion. This work is supported in part by the NSF grant AST-1715246 and NASA grant NNX14AP31G. BL is also supported in part by grants from NSFC (No. 11703068 and No. 11661161012). This work made use of the High Performance Computing Resource in the Core Facility for Advanced Research Computing at Shanghai Astronomical Observatory.

REFERENCES

- Abbott, B. P., Abbott, R., Abbott, T. D., et al. (LIGO Scientific and Virgo Collaboration) 2016a, *PhRvL*, 116, 061102
- Abbott, B. P., Abbott, R., Abbott, T. D., et al. (LIGO Scientific and Virgo Collaboration) 2016b, *PhRvL*, 116, 241103
- Abbott, B. P., Abbott, R., Abbott, T. D., et al. (LIGO Scientific and Virgo Collaboration) 2017a, *PhRvL*, 118, 221101
- Abbott, B. P., Abbott, R., Abbott, T. D., et al. (LIGO Scientific and Virgo Collaboration) 2017b, *ApJL*, 851, L35
- Abbott, B. P., Abbott, R., Abbott, T. D., et al. (LIGO Scientific and Virgo Collaboration) 2017c, *PhRvL*, 119, 141101
- Abbott, B. P., Abbott, R., Abbott, T. D., et al. (LIGO Scientific and Virgo Collaboration) 2017d, *PhRvL*, 119, 161101
- Abbott, B. P., Abbott, R., Abbott, T. D., et al. (LIGO Scientific and Virgo Collaboration) 2018a, arXiv:1811.12907
- Abbott, B. P., Abbott, R., Abbott, T. D., et al. (LIGO Scientific and Virgo Collaboration) 2018b, arXiv:1811.12940
- Anderson, K. R., Storch, N. I., & Lai, D. 2016, *MNRAS*, 456, 3671
- Anderson, K. R., Lai, D., & Storch, N. I. 2017, *MNRAS*, 467, 3066
- Antonini, F., & Perets, H. B. 2012, *ApJ*, 757, 27
- Antonini, F., Toonen, S., & Hamers, A. S. 2017, *ApJ*, 841, 77
- Antonini, F., Rodriguez, C. L., Petrovich, C., & Fischer, C. L. 2018, *MNRAS*, 480, L58
- Banerjee, S., Baumgardt, H., & Kroupa, P. 2010, *MNRAS*, 402, 371
- Barker, B. M., & O’Connell, R. F. 1975, *PhRvD*, 12, 329
- Bartos, I., Kocsis, B., Haiman, Z., et al. 2017, *ApJ*, 835, 165
- Belczynski, K., Dominik, M., Bulik, T., O’Shaughnessy, R., Fryer, C., & Holz, D. E. 2010, *ApJ*, 715, L138
- Belczynski, K., Holz, D. E., Bulik, T., & O’Shaughnessy, R. 2016, *Nature*, 534, 512
- Chatterjee, S., Rodriguez, C. L., Kalogera, V., & Rasio, F. A. 2017, *ApJL*, 836, L26
- Dominik, M., Belczynski, K., Fryer, C., Holz, D. E., Berti, E., Bulik, T., Mandel, I., & O’Shaughnessy, R. 2012, *ApJ*, 759, 52
- Dominik, M., Belczynski, K., Fryer, C., Holz, D. E., Berti, E., Bulik, T., Mandel, I., & O’Shaughnessy, R. 2013, *ApJ*, 779, 72
- Dominik, M., Berti, E., O’Shaughnessy, R., et al. 2015, *ApJ*, 806, 263
- Downing, J. M. B., Benacquista, M. J., Giersz, M., & Spurzem, R. 2010, *MNRAS*, 407, 1946
- Duchêne, G., & Kraus, A. 2013, *ARA&A*, 51, 269
- Fabrycky, D., & Tremaine, S. 2007, *ApJ*, 669, 1298
- Fang, X., Thompson, T. A., & Hirata, C. M. 2018, *MNRAS*, 476, 4234
- Fang, X., Thompson, T. A., & Hirata, C. M. 2019, *ApJ*, 875, 75
- Fragione, G., & Loeb, A. 2019, *MNRAS*, 486, 4443
- Fragione, G., & Kocsis, B. 2019, arXiv:1903.03112
- Fragione, G., Leigh, N., & Perna, R. 2019, arXiv:1903.09160
- Fragione, G., & Bromberg, O. 2019, arXiv:1903.09659
- Gerosa, D., Berti, E., O’Shaughnessy, R., Belczynski, K., Kesden, M., Wysocki, D., & Gladysz W. 2018, *PhRvD*, 98, 084036
- Hamers, A. S., & Lai D. 2017, *MNRAS*, 470, 1657
- Hamers, A. S. 2018, *MNRAS*, 478, 620
- Hoang, B.-M., Naoz, S., Kocsis, B., Rasio, F. A., & Dosopoulou, F. 2018, *ApJ*, 856, 140
- Hoang, B.-M., Naoz, S., Kocsis, B., et al. 2019, *ApJ*, 875, L31
- Kiseleva, L. G., Aarseth, S. J., Eggleton, P. P., & de La Fuente Marcos, R. 1996, in *ASP Conf. Ser. 90, The Origins, Evolution, and Destinies of Binary Stars in Clusters*, ed. E. F. Milone & J.-C. Mermilliod (San Francisco, CA: ASP), 433
- Kobulnicky, H. A., Kiminki, D. C., Lundquist, M. J., et al. 2014, *ApJS*, 213, 34
- Kozai, Y. 1962, *AJ*, 67, 591
- Kremer, K., Rodriguez, C. L., Amaro-Seoane, P., et al. 2019, *PhRvD*, 99, 063003
- Li, G., Naoz, S., Holman, M., & Loeb, A. 2014, *ApJ*, 791, 86
- Lidov, M. L. 1962, *Planetary and Space Science*, 9, 719
- Lithwick, Y., & Naoz, S. 2011, *ApJ*, 742, 94

- Lipunov, V. M., Postnov, K. A., & Prokhorov, M. E. 1997, *AstL*, 23, 492
- Lipunov, V. M., Kornilov, V., Gorbvskoy, E., et al. 2017, *MNRAS*, 465, 3656
- Liu, B., Muñoz, D. J., & Lai, D. 2015, *MNRAS*, 447, 747
- Liu, B., & Lai, D. 2017, *ApJL*, 846, L11
- Liu, B., & Lai, D. 2018, *ApJ*, 863, 68
- Liu, B., & Lai, D. 2019, *MNRAS*, 483, 4060
- Mandel, I., & de Mink, S. E. 2016, *MNRAS*, 458, 2634
- Marchant, P., Langer, N., Podsiadlowski, P., Tauris, T. M., & Moriya, T. J. 2016, *A&A*, 588, A50
- Michaely, E., & Perets, H. B. 2019, arXiv:1902.01864
- Mikkola, S., & Merritt, D. 2008, *AJ*, 135, 2398
- Miller, M. C., & Hamilton, D. P. 2002, *ApJ*, 576, 894
- Miller, M. C., & Lauburg, V. M. 2009, *ApJ*, 692, 917
- Muñoz, D. J., Lai, D., & Liu, B. 2016, *MNRAS*, 460, 1086
- Naoz, S. 2016, *ARA&A*, 54, 441
- O’Leary, R. M., Rasio, F. A., Fregeau, J. M., Ivanova, N., & O’Shaughnessy, R. 2006, *ApJ*, 637, 937
- Peters, P. C. 1964, *Phys. Rev.*, 136, B1224
- Petrovich, C., & Antonini, F. 2017, *ApJ*, 846, 146
- Podsiadlowski, P., Rappaport, S., & Han, Z. 2003, *MNRAS*, 341, 385
- Portegies, Zwart, S. F., McMillan, & S. L. W. 2000, *ApJ*, 528, L17
- Randall, L., & Xianyu, Z.-Z. 2018, *ApJ*, 864, 134
- Randall, L., & Xianyu, Z.-Z. 2019, arXiv:1902.08604
- Rodriguez, C. L., Morscher, M., Pattabiraman, B, et al. 2015, *PhRvL*, 115, 051101
- Rodriguez, C. L., Amaro-Seoane, P., Chatterjee, S., & Rasio, F. A. 2018, *PhRvL*, 120, 151101
- Rodriguez, C. L., & Antonini, F. 2018, *ApJ*, 863, 7
- Samsing, J., & Ramirez-Ruiz, E. 2017, *ApJ*, 840, L14
- Samsing, J., D’Orazio, D. J., Askar, A., & Giersz, M. 2018, arXiv:1802.08654
- Samsing, J., & D’Orazio, D. J. 2018, *MNRAS*, 481, 5445
- Sana, H., de Mink, S. E., de Koter, A., et al. 2012, *Sci*, 337, 444
- Silsbee, K., & Tremaine, S. 2017, *ApJ*, 836, 39
- Stoer, J. 1972, *BAAS*, 4, 422
- Storch, N. I., Anderson, K. R., & Lai, D. 2014, *Sci*, 345, 1317
- Storch, N. I., & Lai, D. 2015, *MNRAS*, 448, 1821
- Thompson, T. A. 2011, *ApJ*, 741, 82
- Venumadhav, T., Zackay, B., Roulet, J., Dai, L., & Zaldarriaga, M. 2019, arXiv:1904.07214
- Wen, L. 2003, *ApJ*, 598, 419
- Zackay, B., Venumadhav, T., Dai, L., Roulet, J., & Zaldarriaga, M. 2019, arXiv:1902.10331
- Zaldarriaga, M., Kushnir, D., & Kollmeier, J. A. 2017, *MNRAS*, 473, 4174
- Zevin, M., Samsing, J., Rodriguez, C., Haster, C.-J., & Ramirez-Ruiz E. 2019, *ApJ*, 871, 91